The Astrophysical Journal, 897:167 (6pp), 2020 July 10 https://doi.org/10.3847/1538-4357/ab980a


# Wave-polarization Analysis of the Alfvénic Slow Solar Wind at Kinetic Scales

Daniele Telloni[1], Roberto Bruno[2], Raffaella D'Amicis[2], Francesco Carbone[3], Rossana De Marco[2], and Denise Perrone[4]

[1] National Institute for Astrophysics—Astrophysical Observatory of Torino Via Osservatorio 20, I-10025 Pino Torinese, Italy; daniele.telloni@inaf.it
[2] National Institute for Astrophysics—Institute for Space Astrophysics and Planetology Via del Fosso del Cavaliere 100, I-00133 Roma, Italy
[3] National Research Council—Institute of Atmospheric Pollution Research c/o University of Calabria, I-87036 Rende, Italy
[4] Italian Space Agency Via del Politecnico snc, I-00133 Roma, Italy
*Received 2020 April 14; revised 2020 May 27; accepted 2020 May 28; published 2020 July 15*

## Abstract

This paper reports the first polarization measurement in the Alfvénic slow solar wind. The normalized magnetic helicity is used as a diagnostic parameter for studying the polarization status of the high-frequency magnetic fluctuations, along with an attempt to identify various wave modes in the solar wind turbulence. Clear evidence for the existence of ion cyclotron waves (ICWs) and kinetic Alfvén waves (KAWs) is also found in the Alfvénic low-speed plasma, robustly supporting the idea that the Alfvénic content of the solar wind fluctuations at fluid scales is the key parameter driving wave generation at kinetic scales. By separating the contributions to helicity from the two modes, it is possible to address the thermodynamical properties of ICWs and KAWs and provide the first direct estimate of their magnetic compressibility. In particular, while ICWs are mainly associated with higher levels of anisotropy and appear to be bounded by the threshold of proton–cyclotron kinetic instability, KAWs (which end up being more compressive than ICWs) are found at lower anisotropies and seem to be limited by the mirror mode instability threshold, extending as well to near the parallel fire hose unstable region. These result are relevant to theories of turbulence and dissipation in the solar wind.

*Unified Astronomy Thesaurus concepts:* Magnetohydrodynamics (1964); Space plasmas (1544); Interplanetary turbulence (830); Alfven waves (23); Solar wind (1534)

## 1. Introduction

The Alfvénic slow solar wind is a stream of magnetized plasma expanding in the heliosphere that, in addition to a self-evident difference in bulk speed, shares with the fast solar wind common characteristics extending from the macrostructure to the microphysics, including ion composition, spectral properties, Alfvénicity (namely the level of correlation between velocity and magnetic field fluctuations), magnetic field compressibility, and amplitude of the embedded fluctuations (D'Amicis et al. 2019, 2020). Their similarity suggests that the Alfvénic low- and high-speed streams have a similar solar origin, namely the polar coronal holes. In particular, while the source of the fast wind has been identified in the core of the coronal holes (Hundhausen 1972), where the solar plasma is accelerated up to 800 km s$^{-1}$ at about 5 $R_\odot$ (Telloni et al. 2007), the Alfvénic slow wind is thought to originate in their peripheral regions, where two mechanisms, in some sense opposite but both related to the geometry of the flux tubes channeling the wind outflows, are likely at work to slow down the expanding coronal plasma to velocities typical of the low-speed streams observed in the heliosphere: the larger superradial divergence of the magnetic field lines (with respect to that characteristic of the core of polar coronal holes, Wang & Sheeley 1990; Abbo et al. 2010) and the areal narrowing of the magnetic flux tubes (Antonucci et al. 2005). In particular, since a larger superradial magnetic field geometry implies a sonic point located at higher heights, this cause the regions adjacent to the coronal holes, where most of the energy deposition would occur below the sonic point, to have a consequent increase of the mass flux rather than the flow speed (as predicted by Leer & Holzer 1980), which thus retains relatively small values (Kopp & Holzer 1976; Levine et al. 1977; Wang & Sheeley 1990; Abbo et al. 2016). On the other hand, the narrowing of the cross section of the flux tubes at the edge of polar coronal holes (that is, surrounding the streamer boundaries) from an initially high areal divergence, can lead to flow stagnation, which has the effect of slowing down the wind relative to a radial flow (Nerney & Suess 2005). On the other hand, recent studies have identified possible sources of the Alfvénic slow solar wind in small coronal holes at low latitudes (Bale et al. 2019; D'Amicis et al. 2019; Wang & Ko 2019; Panasenco et al. 2020). Although the ones mentioned above are the most widely believed scenarios for the generation of slow solar wind with a strong Alfvénic content, coronal streamers (see Abbo et al. 2016, and references therein) and active regions (Zangrilli & Poletto 2012) deserve to be mentioned among the alternative source regions for the typical slow wind.

The discovery of the existence of a slow wind characterized by a high degree of correlation between the velocity $\boldsymbol{V}$ and magnetic field $\boldsymbol{B}$ vectors (the $\boldsymbol{V}$–$\boldsymbol{B}$ correlation) dates back to the early 1980, when Marsch et al. (1981) first identified an Alfvénic low-speed stream at 0.3 au during the perihelion passage of the Helios 2 mission, in a period of low solar activity. However, a statistical and rather comprehensive investigation of the Alfvénic slow wind is to be ascribed to D'Amicis & Bruno (2015) and later on to D'Amicis et al. (2019), Perrone et al. (2020), and Stansby et al. (2020), who provided a detailed characterization of this type of wind (along with its similarities with the fast wind) at both 0.3 and 1 au and during different phases of the solar cycle. The overall properties of the Alfvénic slow wind as outlined in these studies are summarized below.

As far as large scales are considered, the Alfvénic slow wind observed at 1 au clearly resembles the fast wind. Overall, the bulk parameters (an exception is made for the speed and

temperature, which is closer to that assumed by the typical slow wind, but including density and magnetic field intensity, along with their constant trends) are indeed very similar to those found in the main portion of high-speed streams. Moreover, both these Alfvénic solar flows are characterized by a remarkable low magnetic and density compressibility and by the same high level of ***V–B*** correlation, typical of the presence of Alfvénic fluctuations. The Alfvénic slow wind is strongly turbulent ($\delta \boldsymbol{B}/B \sim 1$), with fluctuations as large as those of the fast wind (D'Amicis et al. 2020): this reflects a similar high power level of the spectra at fluid scales. Due to the presence of highly Alfvénic fluctuations, the speed of the Alfvénic slow wind is modulated by the local magnetic field direction, similar to what was experienced by the fast wind (Matteini et al. 2014, 2015). Furthermore, the ion composition of the Alfvénic fast and slow winds, deduced by the ratio of the oxygen ($O^{7+}/O^{6+}$) and carbon ($C^{6+}/C^{5+}$) ions, is similar, suggesting a common coronal source origin, as first pointed out by D'Amicis et al. (2019). Finally, with respect to the typical non-Alfvénic low-speed streams, both the Alfvénic fast and slow winds are characterized by lower values of the collisional age (D'Amicis et al. 2019), indicating that in the younger Alfvénic wind, the lower Coulomb collisions have less effects in isotropizing the cores of ion velocity distributions (Marsch & Goldstein 1983), which can thus preserve their nonthermal features.

The similarities between the Alfvénic slow wind and the fast wind are not limited to the macrostructure; rather they extend also to local microphysics. Both of them occupy approximately the same region in the plasma beta-temperature anisotropy $\beta_\parallel - T_\perp/T_\parallel$ plane ($\beta_\parallel$ is the square of the ratio between the parallel thermal speed and the Alfvén speed), thus suggesting common physical processes underlying the heating of the solar wind plasma at kinetic scales. Also, the small-scale phenomenology of a steeper and steeper slope of the magnetic spectrum at proton scales for a larger and larger power associated with the turbulent Alfvénic fluctuations at fluid scales (first reported by Bruno et al. 2014, for fast streams) is fully recovered also on slower streams as long as they are Alfvénic. Furthermore, as already shown for the fast wind (Bruno & Trenchi 2014), and also in the Alfvénic slow wind, the location of the high-frequency break separating fluid from kinetic scales is well predicted by a cyclotron resonance condition, as first reported by D'Amicis et al. (2019) and later by Duan et al. (2020) on the recent results of the Parker Solar Probe. These last two observational findings are of particular interest since they are both strictly related to the mechanism acting in the solar wind to heat the plasma.

It has been shown on a statistical basis (Telloni et al. 2019) that the amplitude of the Alfvénic fluctuations at fluid scales, rather than the solar wind speed, is the key parameter driving the generation of ion cyclotron waves (ICWs) at kinetic scales through proton–cyclotron instability, triggered by large temperature anisotropies. ICWs can thus be interpreted as the most evident signature of the resonant dissipation of high-frequency Alfvén waves at frequencies near the gyrofrequency $\Omega_p = qB/(m_p c)$ ($q$ and $m_p$ are the proton electric charge and rest mass, respectively, $B$ is the magnetic field intensity, and $c$ is the speed of light). As a matter of fact, He et al. (2019) directly measured the dissipation rate spectrum of the ICWs in the magnetosheath turbulence. Similarly, it is reasonable to assume that the Alfvénicity is the major parameter regulating the signature of the kinetic Alfvén waves (KAWs). As a matter of fact, Bruno & Telloni (2015) provided clues in favor of this conjecture, showing that KAWs are indeed gradually depleted moving, along a high-speed stream, from the more Alfvénic fast wind to the rarefaction region, where the Alfvénicity of the low-frequency fluctuations decreases. Hence, if it were possible to provide evidence for the existence of ICWs and KAWs also in the Alfvénic slow wind, it would be definitely proven that their presence in the solar wind plasma is not related to the nature of the flow (i.e., fast or slow), but rather to its degree of Alfvénicity. It would follow that the generation at kinetic scales of ICWs and KAWs is driven by the solar wind properties at fluid scales, thus supporting previous suggestions by Telloni & Bruno (2016) and Telloni et al. (2019). However, such information is still missing in the present literature: this motivates the investigation of the presence of ICWs and KAWs in the Alfvénic slow solar wind, which is the aim of this paper.

Since ICWs and KAWs are circularly polarized waves with frequencies $\sim\Omega_p$, their identification requires the use of normalized magnetic helicity $\sigma_m$, defined as (Matthaeus et al. 1982; Matthaeus & Goldstein 1982)

$$\sigma_m(\omega) = \frac{2\,\mathrm{Im}[Y^*(\omega)\cdot Z(\omega)]}{E_B}, \tag{1}$$

where $Y$ and $Z$ are the Fourier transforms of the $y$ and $z$ components of $B$ (as a function of the frequency $\omega$), and $E_B$ is the total magnetic spectral energy. The normalized magnetic helicity $\sigma_m$ quantifies indeed the handedness of the magnetic field fluctuations ($\sigma_m = \pm 1$ for right- and left-circularly polarized waves), allowing the characterization of the polarization state of the solar wind parallel and perpendicular fluctuations at proton scales. The data analysis, presented in Section 2, is essentially based on the study of distribution of $\sigma_m$ at kinetic scales as a function of the angle between the solar wind velocity and the local mean magnetic field vectors $\theta_{VB}$, and in the plasma beta-temperature anisotropy $\beta_\parallel - T_\perp/T_\parallel$ and VB angle-magnetic compressibility $\theta_{VB} - C_B$ planes. A discussion of the obtained results, and concluding remarks, are reported in Section 3.

## 2. Analysis and Results

The analysis is performed on the Alfvénic low-speed stream observed at 1 au from 26 to 30 of 2002 January, which was studied by D'Amicis & Bruno (2015) and D'Amicis et al. (2019). Some relevant solar wind parameters relative to this time interval are shown, along with the corresponding average values, in the hatched red area of Figure 1, which altogether extends from 2002 January 22, to February 3. The figure panels display the time profiles of the solar wind speed $V$, the ***V–B*** correlation coefficient $\rho_{VB}$ computed at a 1 hr scale (since this scale is characterized by strong Alfvénic solar wind fluctuations, Bruno et al. 1997), magnetic field intensity $B$, proton number density $n_p$ and temperature $T_p$, total pressure $P$, proton temperature anisotropy $T_\perp/T_\parallel$, and parallel proton plasma beta $\beta_\parallel$. Data come from the Magnetic Field Investigation (MFI) magnetometer (Lepping et al. 1995) and the Solar Wind Experiment (SWE) instruments (Ogilvie et al. 1995) on board the Wind spacecraft, which provide high-resolution 11 Hz magnetic field measurements and 92 s resolution moments from proton velocity distribution functions, respectively.

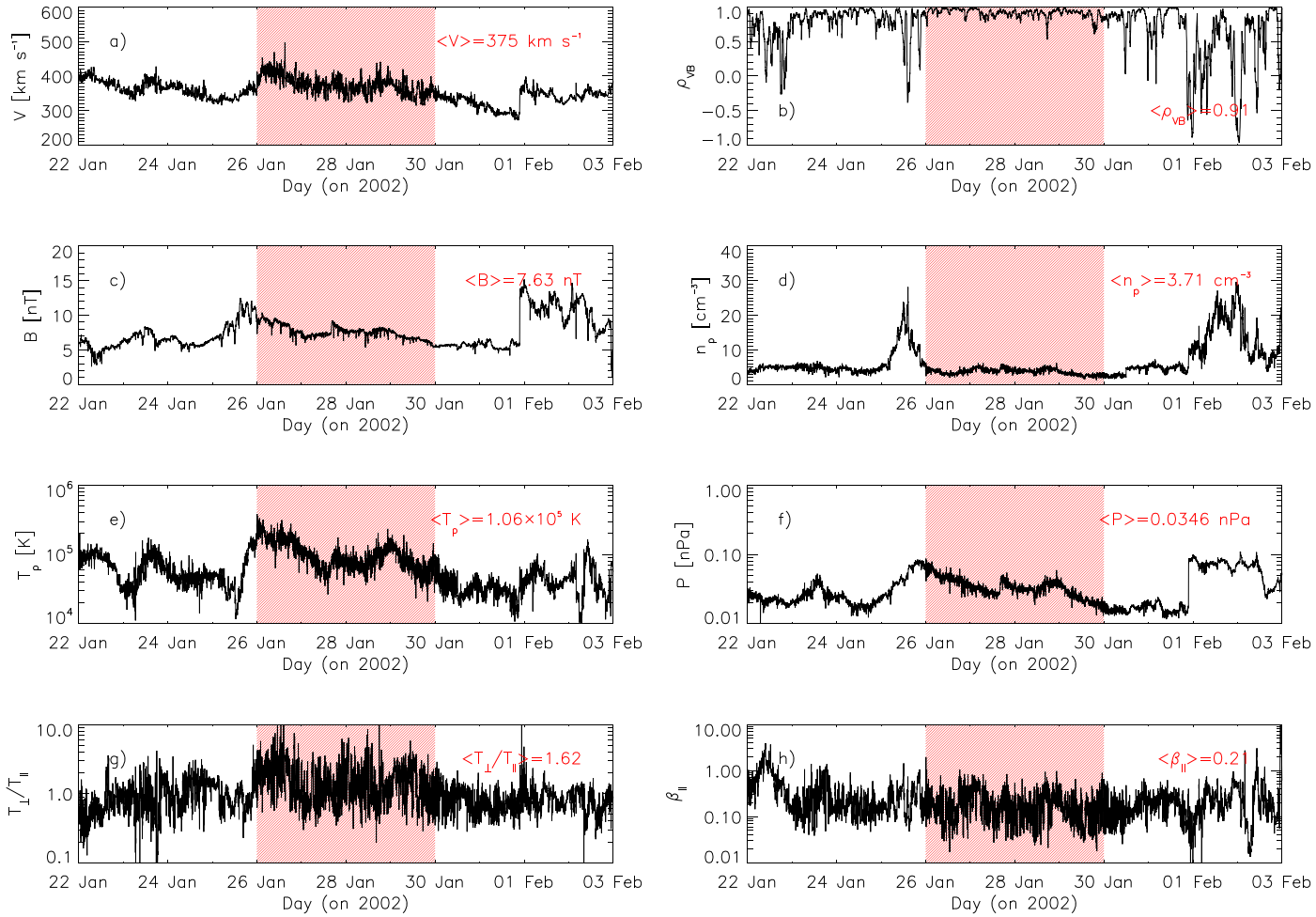


**Figure 1.** Time series of solar wind speed (*a*), ***V–B*** correlation coefficient (*b*), magnetic field intensity (*c*), proton number density (*d*) and temperature (*e*), total pressure (*f*), proton temperature anisotropy (*g*), and parallel proton plasma beta (*h*), over the period from 2002 January 22, to February 3; the hatched red area highlights the Alfvénic low-speed stream under study; the corresponding average values of the solar wind parameters are reported in each panel.

Although the large-scale properties of this Alfvénic slow flow have been exhaustively described in the previous studies by D'Amicis & Bruno (2015) and D'Amicis et al. (2019), it is worth recalling its main characteristics as outlined by Figure 1. The ***V***- ***B*** correlation coefficient $\rho_{VB}$, which quantifies the Alfvénic content of the solar wind fluctuations, retains very high values along the whole low-speed stream ($\langle\rho_{VB}\rangle = 0.91$), thus robustly indicating the presence of Alfvénic fluctuations (panel (b)). As expected for Alfvénic flow streams, also this Alfvénic time period is characterized by enhanced velocity fluctuations, and by low compression in both magnetic field intensity and proton number density (panels (a), (c) and (d), respectively). The temperature and pressure observed within the Alfvénic slow flow are larger than those in the upstream and downstream regions (panels (e) and (f), respectively), likely indicating that the flux-tube expansion factor is larger with respect to the surrounding plasma, in accordance with the superradial expansion as the major mechanism responsible for the lower speeds. Finally, a low level of temperature anisotropy ($\langle T_\perp/T_\parallel\rangle = 1.62$) and a plasma-magnetic pressure imbalance ($\langle\beta_\parallel\rangle = 0.21$) are observed (panels (g) and (h), respectively). In particular, these last two parameters are very important (since they allow the description of the thermodynamical state of the plasma) and will be used to investigate of the nature of the polarized magnetic fluctuations at proton scales.

In order to search for the existence of ICWs and KAWs in the Alfvénic slow wind, the approach of using the normalized magnetic helicity $\sigma_m$ to diagnose the wave-polarization characteristics of the magnetic field fluctuations (first introduced by He et al. 2011; Podesta & Gary 2011) is adopted in this work. It is based on the estimation of the $\theta_{VB}$ distribution of $\sigma_m$ at every frequency and on the search for populations of field-aligned (highly oblique) fluctuations with an intrinsic negative (positive) magnetic helicity sign ($\sigma_m \lessgtr 0$), at frequencies near the gyrofrequency $\Omega_p$, which can be interpreted as parallel-(perpendicular-) propagating left-(right-)handed polarized ICWs (KAWs). More details on this analysis technique can be found in the literature (e.g., He et al. 2011; Podesta & Gary 2011; Bruno & Telloni 2015; Telloni et al. 2015).

The results of this polarization analysis are shown in Figure 2, which displays the distribution of the normalized magnetic helicity $\sigma_m$ as a function of the local VB angle and frequency.

Two strongly and oppositely polarized magnetic populations are clearly resolved just below the proton–cyclotron resonance frequency $\Omega_p$ (dashed line in Figure 2), at quasi-perpendicular and quasi-parallel directions. Since the magnetic sector observed during the selected time interval is inwardly oriented, the positive (negative) magnetic helicity excesses shown in the

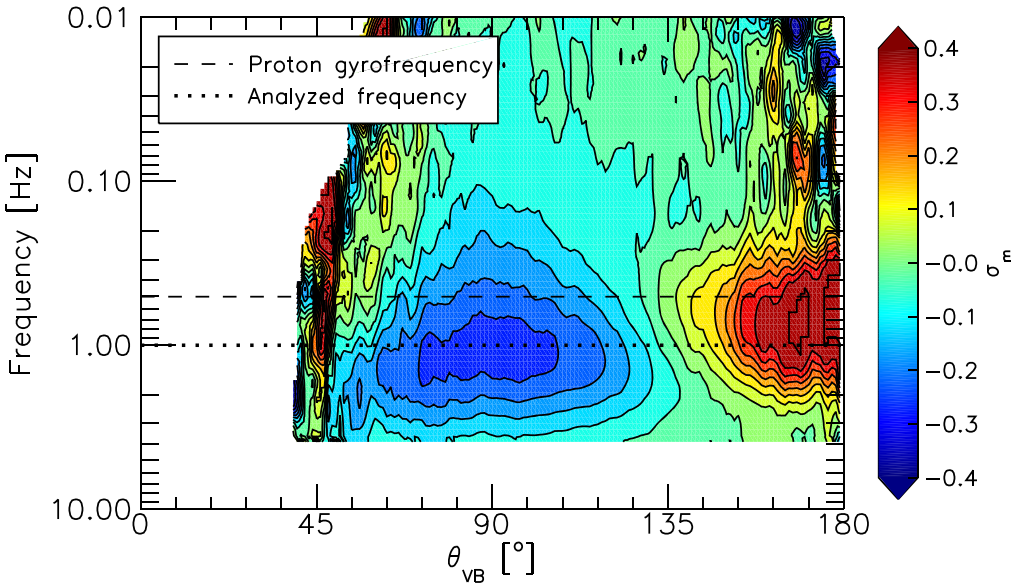


**Figure 2.** Distribution of the normalized magnetic helicity $\sigma_m$ spectrum with respect to the $\theta_{VB}$ angle between the flow direction and the local mean magnetic field; the frequency corresponding to the proton–cyclotron resonance condition and that selected for analyzing the nature of the polarized fluctuations at proton scales (see the text for details) are shown as a dashed and dotted line, respectively.

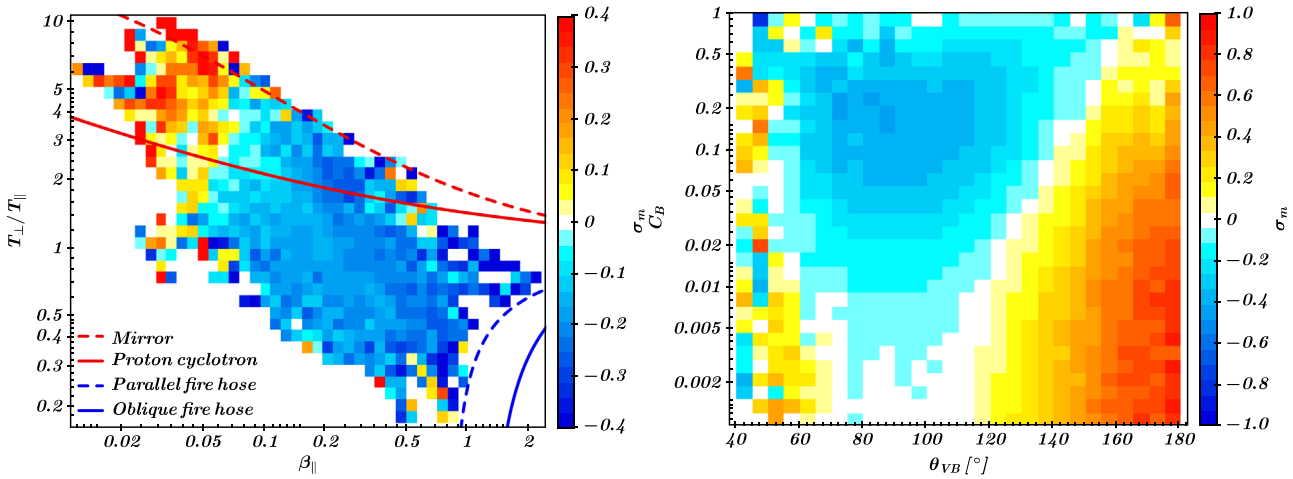


**Figure 3.** 2D histogram of the median value of the normalized magnetic helicity $\sigma_m$ in the $\beta_\parallel - T_\perp/T_\parallel$ (left) and $\theta_{VB} - C_B$ (right) spaces; the mirror, proton, and parallel and oblique fire hose instabilities are also reported in the $\beta_\parallel - T_\perp/T_\parallel$ plane as lines with different styles.

$\sigma_m$ angular distribution, correspond to left- and right-handed polarized fluctuations, which are respectively propagating roughly along and across the local magnetic field. These magnetic fluctuations are commonly interpreted as due to KAWs and ICWs (He et al. 2011; Podesta & Gary 2011; Bruno & Telloni 2015; Telloni et al. 2015; Telloni & Bruno 2016), which thus also exist also Alfvénic slow wind. Quite interestingly, as already noticed in Telloni et al. (2015) and Bruno & Telloni (2015) for the fast wind, in the Alfvénic slow wind the core of the ICW population is also located at lower frequencies with respect to that of KAWs, which have a larger frequency extend.

In order to characterize in more detail the two families of magnetic fluctuations that comprise the selected Alfvénic low-speed stream, the contribution to normalized magnetic helicity from ICWs and KAWs is separated by studying the distribution of $\sigma_m$ in the plasma beta-temperature anisotropy $\beta_\parallel - T_\perp/T_\parallel$ and in the VB angle-magnetic compressibility $\theta_{VB} - C_B$ spaces. In order to accomplish this task, the frequency of 1 Hz, which runs close to the cores of the two oppositely polarized populations (dotted line in Figure 2) and thus allows the capture of both ICWs and KAWs, is considered in the analysis. The left and right panels of Figure 3 show the median values of $\sigma_m$ at 1 Hz in the $\beta_\parallel - T_\perp/T_\parallel$ and $\theta_{VB} - C_B$ parameter planes, respectively. The four plasma instabilities driven by proton temperature anisotropy (as adapted from Hellinger et al. 2006, for a constant maximum growth rate $\gamma \sim 10^{-3}\Omega_p$) are displayed in the $\beta_\parallel - T_\perp/T_\parallel$ space with different line types.

As highlighted in D'Amicis et al. (2019), when the Alfvénic low-speed stream of 2002 January is studied as a whole, the plasma is on average in a thermodynamical state characterized by an almost thermal equilibrium ($T_\perp/T_\parallel \sim 1$) and by low beta values ($\beta_\parallel \sim 0.3$). Furthermore, overall a very low compressibility is exhibited by the magnetic fluctuations, as expected for highly Alfvénic intervals (Bruno & Bavassano 1991). However, the separation of the ICWs and KAWs on the basis of their polarization makes it possible to estimate their correlation with the thermodynamical state of plasma and their

compressibility level. The two populations are clearly distinguishable in both the $\beta_{\parallel} - T_{\perp}/T_{\parallel}$ and $\theta_{VB} - C_B$ planes. ICWs are found at high temperature anisotropies ($T_{\perp}/T_{\parallel} \gtrsim 3$) and very low beta plasma values ($\beta_{\parallel} \lesssim 0.07$), which is de facto in a region unstable with respect to the proton–cyclotron instability (as already reported by Telloni et al. 2015, 2019, for the fast wind). On the other hand, KAWs are distributed in a much larger region of the $\beta_{\parallel} - T_{\perp}/T_{\parallel}$ space, where $\beta_{\parallel}$ is generally smaller than 0.1 and $T_{\perp}/T_{\parallel}$ mostly lower than 1. The wide intervals of $T_{\perp}/T_{\parallel}$ and $\beta_{\parallel}$ values spanned by KAWs might indicate that these fluctuations are somehow insensitive to proton temperature anisotropy, in agreement with Klein & Howes (2015). However, KAWs seem to be possibly limited by the parallel fire hose instability (blue dashed line in the left panel of Figure 3), which can thus be suggested to play some role in driving modes with a right-handed helicity, even if no definitive conclusions can be drawn only on the basis of the present analysis. Indeed, there is currently no theory predicting that KAWs are directly excited by the fire hose instability. At fluid scales, the fire hose instability can be responsible for the generation of Alfvén waves, as reported, for instance, by He et al. (2018) in the magnetic reconnection exhaust regions, where enhanced Alfvénic turbulence has been observed in relation to fire hose unstable energized plasmas. At kinetic scales, it is predicted that the fire hose instability drives quasi-parallel propagating and right-handed polarized wave modes, thus interpreted as magnetosonic/whistler waves (e.g., Podesta & Gary 2011). On the other hand, KAWs may be excited by electron current instability or energetic ion beam instability (Voitenko 1998; Chen et al. 2013). Furthermore, observations show that KAWs lie inside the region unstable with respect to the proton–cyclotron instability and seem to be bounded also by the mirror mode instability threshold (red solid and dashed lines in the left panel of Figure 3, respectively). Therefore, which plasma instability is crucial in driving KAWs or whether more instabilities may be at play at the same time are still open questions, which require further observational and theoretical investigation to be tackled.

In addition, this technique allows, for the first time, the estimation of the compressive character of ICWs and KAWs. In fact, the right panel of Figure 3 indicates that right-handed polarized fluctuations ($\sigma_m < 0$) propagating at $\theta_{VB} \sim 90°$ have a compressive ratio $C_B = (\sigma_B^2/\sum_{i=x,y,z}\sigma_{B_i}^2)^{1/2}$ (with $\sigma_B^2$ and $\sigma_{B_i}^2$ as the variances of the magnetic field intensity and components, respectively, computed over 1 second) of about 0.1 or more, while parallel-propagating left-handed polarized fluctuations ($\sigma_m > 0$) exhibit much lower values ($C_B \lesssim 0.01$). Thus, KAWs are largely more compressive than ICWs. In fact, as the wavevector $\boldsymbol{k}$ becomes relatively more and more oblique to the background magnetic field, compressibility increases consequently. Thus, it is experimentally confirmed that most of the compressive character of the fluctuations at proton kinetic scales (e.g., Hollweg 1999; Alexandrova et al. 2008; Podesta 2013; Telloni et al. 2015, and many others) is due to the presence of KAWs.

## 3. Discussion and Conclusions

The results outlined in the previous section show that ICWs and KAWs also populate the slow wind as long as it is characterized by a high degree of Alfvénic correlations. Hence, the presence of Alfvén waves in the inertial range is a *sine qua non* condition for the existence of both these types of waves at kinetic scales in the solar wind turbulence. This is further evidence that the solar wind should be classified according to its Alfvénicity level, rather than its speed. In other words, the classic distinction between fast and slow wind should be revised in Alfvénic and not Alfvénic streams. Indeed, as exhaustively shown by D'Amicis et al. (2019), the Alfvénic slow wind shares more characteristics with the fast wind than with the typical, not Alfvénic slow flow. This paper extends their similarities to the thermodynamical properties of ICWs and KAWs. A comparison of the left panel of Figure 3 with Figure 3 reported in Telloni & Bruno (2016) clearly reveals that in both fast and slow Alfvénic solar wind regimes, ICWs occupy approximately the same region in the $\beta_{\parallel} - T_{\perp}/T_{\parallel}$ parameter space, at $T_{\perp}/T_{\parallel} > 1$ and $\beta_{\parallel} < 1$, exhibiting a higher temperature anisotropy and a lower parallel plasma beta with respect to KAWs. Similarly, KAWs are mainly located around $T_{\perp}/T_{\parallel} \sim 1$ and $\beta_{\parallel} \sim 1$ in both wind types.

Although some clues were already provided by Telloni et al. (2015), this paper reports the first experimental assessment of the compressibility level of ICWs and KAWs, with the latter being much more compressive than the former. The low (high) magnetic compressibility exhibited by $k_{\parallel}$ ($k_{\perp}$) fluctuations at frequencies around $\Omega_p$ reinforces their interpretation in terms of ICWs and KAWs, respectively. As turbulence develops for $\boldsymbol{k}_{\perp}$, Alfvénic fluctuations at kinetic scales have very oblique wavevectors and are hence very compressive. Thus, as a further result, this paper observationally supports theoretical models predicting that high-frequency magnetic fluctuations in a low-beta solar wind plasma mainly arise from a spectrum of KAWs (Howes et al. 2008; Schekochihin et al. 2009).

D.T. and R.D.M. were partially supported by the Italian Space Agency (ASI) under contract I/013/12/0. Wind data were downloaded from the NASA-CDAWeb.

## ORCID iDs

Daniele Telloni https://orcid.org/0000-0002-6710-8142
Roberto Bruno https://orcid.org/0000-0002-2152-0115
Raffaella D'Amicis https://orcid.org/0000-0003-2647-117X
Francesco Carbone https://orcid.org/0000-0002-3559-5273
Rossana De Marco https://orcid.org/0000-0002-7426-7379
Denise Perrone https://orcid.org/0000-0003-1059-4853

## References

Abbo, L., Antonucci, E., Mikić, Z., et al. 2010, AdSpR, 46, 1400
Abbo, L., Ofman, L., Antiochos, S. K., et al. 2016, SSRv, 201, 55
Alexandrova, O., Carbone, V., Veltri, P., & Sorriso-Valvo, L. 2008, ApJ, 674, 1153
Antonucci, E., Abbo, L., & Dodero, M. A. 2005, A&A, 435, 699
Bale, S. D., Badman, S. T., Bonnell, J. W., et al. 2019, Natur, 576, 237
Bruno, R., & Bavassano, B. 1991, JGR, 96, 7841
Bruno, R., Bavassano, B., Pietropaolo, E., Carbone, V., & Rosenbauer, H. 1997, JGR, 102, 14687
Bruno, R., & Telloni, D. 2015, ApJL, 811, L17
Bruno, R., & Trenchi, L. 2014, ApJL, 787, L24
Bruno, R., Trenchi, L., & Telloni, D. 2014, ApJL, 793, L15
Chen, L., Wu, D. J., & Huang, J. 2013, JGRA, 118, 2951
D'Amicis, R., & Bruno, R. 2015, ApJ, 805, 84
D'Amicis, R., Matteini, L., & Bruno, R. 2019, MNRAS, 483, 4665
D'Amicis, R., Matteini, L., Bruno, R., & Velli, M. 2020, SoPh, 295, 46
Duan, D., Bowen, T. A., Chen, C. H. K., et al. 2020, ApJS, 246, 55
He, J., Duan, D., Wang, T., et al. 2019, ApJ, 880, 121
He, J., Marsch, E., Tu, C., Yao, S., & Tian, H. 2011, ApJ, 731, 85
He, J., Zhu, X., Chen, Y., et al. 2018, ApJ, 856, 148

Hellinger, P., Trávníček, P., Kasper, J. C., & Lazarus, A. J. 2006, GeoRL, 33, L09101
Hollweg, J. V. 1999, JGR, 104, 14811
Howes, G. G., Dorland, W., Cowley, S. C., et al. 2008, PhRvL, 100, 065004
Hundhausen, A. J. 1972, Coronal Expansion and Solar Wind (Berlin: Springer)
Klein, K. G., & Howes, G. G. 2015, PhPl, 22, 032903
Kopp, R. A., & Holzer, T. E. 1976, SoPh, 49, 43
Leer, E., & Holzer, T. E. 1980, JGR, 85, 4681
Lepping, R. P., Acũna, M. H., Burlaga, L. F., et al. 1995, SSRv, 71, 207
Levine, R. H., Altschuler, M. D., Harvey, J. W., & Jackson, B. V. 1977, ApJ, 215, 636
Marsch, E., & Goldstein, H. 1983, JGR, 88, 9933
Marsch, E., Rosenbauer, H., Schwenn, R. R., Muehlhaeuser, K.-H., & Denskat, K. U. 1981, JGR, 86, 9199
Matteini, L., Horbury, T. S., Neugebauer, M., & Goldstein, B. E. 2014, GeoRL, 41, 259
Matteini, L., Horbury, T. S., Pantellini, F., Velli, M., & Schwartz, S. J. 2015, ApJ, 802, 11
Matthaeus, W. H., & Goldstein, M. L. 1982, JGR, 87, 6011
Matthaeus, W. H., Goldstein, M. L., & Smith, C. 1982, PhRvL, 48, 1256
Nerney, S., & Suess, S. T. 2005, ApJ, 624, 378
Ogilvie, K., Chornay, D., Fritzenreiter, R., et al. 1995, SSRv, 71, 55
Panasenco, O., Velli, M., D'Amicis, R., et al. 2020, ApJS, 246, 54
Perrone, D., D'Amicis, R., de Marco, R., et al. 2020, A&A, 633, A166
Podesta, J. J. 2013, SoPh, 286, 529
Podesta, J. J., & Gary, S. P. 2011, ApJ, 734, 15
Schekochihin, A. A., Cowley, S. C., Dorland, W., et al. 2009, ApJS, 182, 310
Stansby, D., Matteini, L., Horbury, T. S., et al. 2020, MNRAS, 492, 39
Telloni, D., Antonucci, E., & Dodero, M. A. 2007, A&A, 472, 299
Telloni, D., & Bruno, R. 2016, MNRAS, 463, L79
Telloni, D., Bruno, R., & Trenchi, L. 2015, ApJ, 805, 46
Telloni, D., Carbone, F., Bruno, R., et al. 2019, ApJL, 885, L5
Voitenko, Yu. M. 1998, JPlPh, 60, 497
Wang, Y.-M., & Ko, Y.-K. 2019, ApJ, 880, 146
Wang, Y.-M., & Sheeley, N. R., Jr. 1990, ApJ, 355, 726
Zangrilli, L., & Poletto, G. 2012, A&A, 545, A8